Density-functional theory study of polarization saturation in strained ferroelectrics

Yanpeng Yao and Huaxiang Fu
Department of Physics, University of Arkansas, Fayetteville, Arkansas 72701, USA
(Received 24 June 2009; published 24 July 2009)

Using density-functional calculations and the modern theory of polarization, we study the structure and polarization responses of tetragonal $PbTiO_3$, $BaTiO_3$, and $SrTiO_3$ in a strain regime that is previously overlooked. We find that the χ_3 polarizations in all three substances saturate at large strains, revealing a phenomenon that is generally applicable. The saturation demonstrates the existence of a sophisticated collective behavior in the large-strain regime and is shown to originate possibly from electron-ion correlation that leads to a cancellation between electronic and ionic polarizations. Our results shed insight on the polarization properties and provide explanations for the puzzling results recently observed in experiments.

DOI: 10.1103/PhysRevB.80.035126 PACS number(s): 77.22.Ej, 77.65.−j, 77.80.−e

I. INTRODUCTION

Response of electric polarization to external strains in infinite solids is a subject of considerable importance from both fundamental and technological points of view.[1–3] Spread interest has been generated to understand the direct physics and/or mechanism underlying the response.[4–8] Fundamentally, the process is governed by electrons, ions, and their complex interactions, forming an important class of collective phenomena. Previously, Ederer and Spaldin[4] showed that the strain effects on polarization depend strongly on materials and could be understood by the piezoelectric and elastic constants of the unstrained materials. In a recent study, the polarization in a highly strained $Pb(Zr_{0.2}Ti_{0.8})O_3$ (PZT) film (with $c/a \approx 1.09$) was found to be similar to that in a relaxed PZT film (with $c/a \approx 1.05$), showing a surprisingly weak strain dependence.[5] Technologically, in-plane compressive strains were demonstrated to be able to dramatically raise the critical Curie temperature by 500 °C in $BaTiO_3$ (Ref. 6) and to turn incipient $SrTiO_3$ into strongly ferroelectric.[7,8] These important studies focus on small strains near equilibrium.

Nowadays, advancement in fabrication of various high-quality ferroelectric (FE) nanostructures[9] (such as films, wires, and dots) opens an opportunity for studying polarization response in a new regime with medium and/or large strains that thus far received little attention.[10] Unlike bulks, FE wires or dots can allow exceeding (external) strains without formation of dislocation since stress can be effectively relaxed due to finite lateral size.[11] For instance, large compressive strains can be realized in FE nanorods[12] by compressing them along the lateral directions. Even for thin films, strains of more than 3% were shown possible in $LaAlO_3/SrTiO_3$.[13] This large strain regime is interesting and may possibly reveal notable physics since the charge density is heavily deformed by large strains, making electrons behave more collectively in some spatial region but less in another. As a result, answers to questions (1) what structural properties FEs may display in this regime and (2) how polarization, as a collective phenomenon, adjusts itself to large strains, remain largely unknown. Furthermore, scientists have been long wondering what is the upper limit that polarization is able to reach, provided that exceeding strain is possible in laboratory.[14] This is a rather intriguing question since the limit (if exists) defines a profound constraint that polarization can be enhanced by mechanical strain.

Polarization in periodic solids can be expressed in lattice-vector coordinate as $\mathbf{P}=\frac{e}{\Omega}(\chi_1\mathbf{a}_1+\chi_2\mathbf{a}_2+\chi_3\mathbf{a}_3)$, where Ω is the volume of a unit cell and χ_i describes the polarization along the direction of lattice vector $\mathbf{a}_i$. When in-plane strains are imposed, polarization is to be altered because of (1) the variation in χ_i and (2) the cell-structure modifications of Ω and $\mathbf{a}_i$. The first factor is more important and is manifested[15,16] in the *proper* piezoelectric coefficients as $e^{\mathrm{pro}}_{\alpha\beta\gamma}=\frac{e}{\Omega}\Sigma_i\frac{d\chi_i}{d\epsilon_{\beta\gamma}}a_{i\alpha}$, where $\epsilon_{\beta\gamma}$ is the strain in Cartesian notation and α, β, and γ are indices for Cartesian directions. The second factor merely contributes to the *improper* piezoelectric coefficient which is trivially related to the proper coefficient by $e^{\mathrm{impro}}_{\alpha\beta\gamma}=e^{\mathrm{pro}}_{\alpha\beta\gamma}+\delta_{\alpha\beta}P_\gamma-\delta_{\beta\gamma}P_\alpha$. One thus notes that χ_i is the key quantity that is technologically relevant in terms of obtaining high piezoelectric coefficients. Our study will be concerned with the strain dependence of χ_i.

Here by means of first-principles calculations we investigate the structure and polarization responses of FE perovskites in the large strain regime. Three paradigm materials—namely, $PbTiO_3$ (PT), $BaTiO_3$ (BT), and $SrTiO_3$ (ST)—are studied, aimed to draw conclusions that are generally applicable. We find that these perovskites all exhibit *three* distinct stages (I, II, and III) in their structural and polarization responses. Different from stage I of small strain (which has been extensively studied in the literature), strongly enhanced ferroelectric off-center displacements and large tetragonality are predicted to take place in stage II. Interestingly, these enhancements disappear in stage III despite the in-plane strain is even higher. However, another unusual phenomenon occurs, that is, the in-plane strain ceases to play a role in affecting the χ_3 polarization in stage III. In fact, our calculations predict the existence of a critical in-plane strain above which χ_3 starts to saturate.

Three considered materials represent FEs of different magnitudes of polarization: PT is strongly ferroelectric, BT is ferroelectric but with a weaker polarization, and ST is not FE under zero strain. We study the structural phase of tetragonal symmetry ($|\mathbf{a}_1|=|\mathbf{a}_2|=a$ and $|\mathbf{a}_3|=c$). Biaxial compressive strains are applied on the $\mathbf{a}_1$-$\mathbf{a}_2$ plane and are defined in the Voigt notation as $\eta_1=\eta_2=(a_0-a)/a_0$, where a_0 is the

unstrained in-plane lattice constant. The oxygen-octahedra rotation is also considered for ST. Our system under biaxial in-plane strain is different from that in Ref. 17 (where PT is expanded along all three directions by negative hydrostatic pressure) and from the PT thin films under external electric fields in Ref. 18 (in which the in-plane lattice constant is fixed at the value of ST substrate). Our system also differs from the one studied by Duan *et al.*[10] where the σ_{33} stress is nonzero for each calculated data point while in our work, σ_{33} vanishes for every fixed in-plane strain. The *stress*-dependent polarization behavior in Ref. 10 thus does not hold here. As a matter of fact, none of the previous studies[10,17,18] have revealed the saturation of the χ_3 polarization.

II. THEORETICAL METHOD

We use density-functional theory within the local-density approximation (LDA)[19] to determine optimized cell shape and atomic positions by minimization of total energy. Calculations are performed using a pseudopotential approach with mixed-basis set[20] in which numerical atomic pseudo-orbitals and a sufficient number of plane waves are employed as bases to expand the Bloch wave functions. Core electrons are replaced by the Troullier-Martins type of pseudopotentials;[21] semicore states of Ti $3s$ and $3p$ are included in the calculations as valence states. Atomic configurations for pseudopotential generation, pseudo/all-electron matching radii, and accuracy checking were described elsewhere.[22] A cutoff energy of 100 Ry is used for all three substances and is found to be sufficient. Atomic relaxations are performed until the residual forces on individual atoms are less than 10^{-3} eV/Å. A unit cell consists of 5 atoms for strained FEs when there is no oxygen rotation and 10 atoms for strained FEs with oxygen rotation. Our theoretical in-plane lattice constants of unstrained bulks (a_0=3.88 Å for PT, a_0=3.95 Å for BT, and a_0=3.86 Å for ST) agree well with other existing calculations.

Displacement of ions and deformation of electron density both contribute to polarization. Computing of ionic contribution (labeled as $\mathbf{P}_{\text{ion}}$) is straightforward using point charges while electronic contribution (denoted as $\mathbf{P}_{\text{el}}$) is determined using the modern theory of polarization,[23,24] as implemented in our mixed-basis method. More specifically, $\mathbf{P}_{\text{el}}$ is computed as the geometrical Berry phase of valence-electron states as $\mathbf{P}_{\text{el}}=i\frac{2e}{(2\pi)^3}\int d\mathbf{k}_1\nabla_{\mathbf{k}_2}\phi(\mathbf{k}_1,\mathbf{k}_2)|_{\mathbf{k}_1=\mathbf{k}_2}$, where $\phi(\mathbf{k}_1,\mathbf{k}_2)=\ln\det|\langle u_{m\mathbf{k}_1}|u_{n\mathbf{k}_2}\rangle|$ is the phase of the determinant formed by occupied Bloch wave functions $u_{n\mathbf{k}}$.

III. STRUCTURAL RESPONSE

At zero strain, ST undergoes an antiferrodistortive oxygen rotation at 105 K but this rotation does not exist in PT and BT. To facilitate the comparison among three materials, we first consider no oxygen rotation in these FEs. Later in Sec. VI, rotation of oxygen octahedra is taken into account for both unstrained and strained ST. When there is no rotation of oxygen octahedra, Fig. 1(a) depicts the calculated c/a tetragonalities for three considered materials under compressive strains. Let us study the BT curve first. For this curve, (1) our

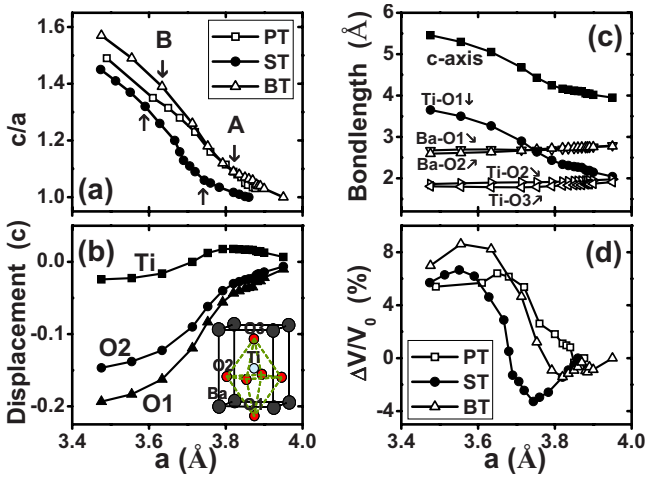

FIG. 1. (Color online) Structural properties as a function of in-plane lattice constant: (a) the c/a tetragonalities (where points A and B are marked by arrows only for BT and ST, for the sake of the clarity of display); (b) atomic displacements (in units of c) in BT; (c) bond lengths in BT (where the c-axis length is also plotted for comparison); (d) the change in cell volume $\Delta V/V_0$ (V_0 is the equilibrium volume). Labels of individual atoms in the tetragonal perovskite are given in the inset of (b).

calculations confirm the (expected) linear relation between c/a and a when in-plane strain is small; (2) however, as the in-plane a length is decreased to 3.82 Å [marked as point A in Fig. 1(a)], BT apparently enters a different state, as witnessed by the fact that the c/a ratio rises more sharply afterward; (3) interestingly, when a reaches point B, the c/a becomes nearly linear again despite the in-plane strain is even higher [in fact, more data points that are not shown in Fig. 1(a) have been calculated at $a<3.4$ Å and confirmed the linearity]. Combination of these results makes the tetragonality in the region between A and B considerably enhanced.

Comparison of three materials in Fig. 1(a) tells us that the above conclusions are valid also for PT and ST. But the c/a value and the location of the threshold point A reveal some interesting differences. First, for a fixed in-plane lattice constant, BT is predicted to exhibit a larger (not smaller) c/a tetragonality than PT, unlike the zero-strain case. Meanwhile, the c/a ratio in ST is the least, and is significantly lower than that in BT or PT. Second, the critical in-plane lattice constant at point A is similar for PT and BT but not for ST. We attribute this to the small size of Sr atom. When strained, the big Ba or Pb atoms repel other atoms more forcefully, leading to the earlier occurrence of point A.

We next examine the atomic off-center displacements in strained BT [Fig. 1(b)], obtained by placing the Ba atom at the cell origin and then determining the displacements of Ti, O1, and O2 atoms with respect to their high-symmetry locations. Labels of individual atoms are given in the inset of Fig. 1(b). We see in Fig. 1(b) that the oxygen off-center displacements alter dramatically from the right side of the A point (where the slope of the displacement curve is small) to the left side of the A point (where the slope of the displacement curve is steep), explaining why point A plays an important role. Between A and B, the O1 and O2 displacements are

shown to be sensitive to—and are thus markedly tunable by—the lattice misfit. This sensitivity is far better than in the small-strain regime. Figure 1(b) also reveals that when $a > a_A$ the Ti atom shifts up (out of phase with the downward O displacements) and then begins to move down (in phase with the O displacements) for $a < a_A$. Given the complex interplay between atomic displacements and the c/a tetragonality, it would be useful to seek a mechanism (if any) that may govern how, and by what magnitude, atoms are displaced in strained ferroelectrics. We find that such a mechanism indeed exists and is manifested in the bond lengths in Fig. 1(c). Two observations are ready in Fig. 1(c): (1) the Ti-O1 bond distance correlates well with the c length and (2) despite the fact that the in-plane lattice constant is compressed by as much as ~0.5 Å, the Ti-O2 and Ti-O3 bond lengths nevertheless maintain to be almost constant (so are the Ba-O1 and Ba-O2 bond lengths). Our calculations thus reveal a simple rule that can quantitatively explain the structural response *over a wide range* of in-plane strains, namely, FEs respond to the substrate misfit strain in a manner that maintains the lengths of short Ti-O and Ba-O bonds. This rule is found true also for PT and ST and shall be verifiable in x-ray experiments.

However, FE perovskites do not maintain the bond lengths in a trivial way. In Fig. 1(d) we describe the strain dependence of the optimal cell volume. Cell volume is often assumed to be constant under biaxial strains. This is not the case in Fig. 1(d). Instead, Fig. 1(d) displays features that are very suggestive. Under small strains, the cell volume first decreases and this decrease is most pronounced in ST. Then approximately at a_A, the volume of the material starts to expand drastically, by more than 8% in BT, and later at a_B, it starts to decrease again. One thus sees that between a_A and a_B the enhanced c/a in Fig. 1(a)—and the enlarged O displacements in Fig. 1(b)—occur by the interesting expansion of cell volume. The characteristic nonmonotonous change in cell volume found in our study is thus different from the volume response in PT under external c-axis stress,[10] where the volume was shown to increase monotonously.

IV. POLARIZATION RESPONSE

Figure 2(a) depicts the χ_3 polarization and the proper $e_{31}^{\text{pro}} \equiv -\frac{e}{\Omega}\frac{d\chi_3}{d\eta_1}c$ piezoelectric coefficient in PT under varied compressive strains. Caution is made to ensure that we follow continuously the same polarization as χ_3 crosses different branches since polarization in periodic solids is intrinsically a multivalued quantity. At zero strain, PT shows a theoretical χ_3 value of 0.63, which corresponds to a polarization of 66.7 $\mu C/cm^2$, consistent with the experimental result of ~70 $\mu C/cm^2$.[25] Upon strain, PT displays three stages—labeled as I, II, and III in Fig. 2(a)—in its polarization response. Point A in Fig. 1(a) separates stages I and II while point B separates stages II and III. At stage I ($a > 3.84$ Å), the χ_3 polarization increases linearly, from which the piezoelectric e_{31}^{pro} coefficient is deduced to be 637 $\mu C/cm^2$. At stage II, the linear $\chi_3 \sim a$ relation remains but with a different slope from that of stage I. The e_{31}^{pro} value for stage II is 898 $\mu C/cm^2$. As the in-plane strain continuously varies from stage I to II, we notice an abrupt rise in the polarization, leading to the occurrence of a giant e_{31}^{pro} coefficient of 3900 $\mu C/cm^2$ near $a = 3.84$ Å.

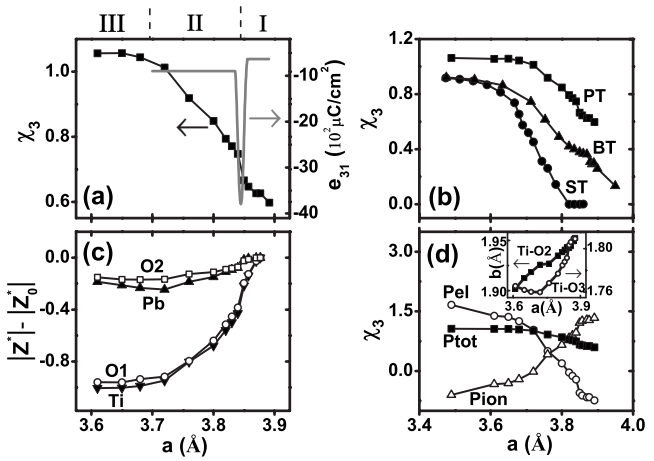

FIG. 2. Dependencies of the following properties as a function of the in-plane lattice constant: (a) the χ_3 component of polarization (using the left vertical axis) and piezoelectric e_{31}^{pro} coefficient (using the right vertical axis) in PT, (b) the χ_3 polarizations in BT and ST, compared to that in PT, (c) effective charges $|Z^*| - |Z_0^*|$ in PT, and (d) electronic (P_{el}) and ionic (P_{ion}) contributions to the total (P_{tot}) polarization in PT. For each calculated point in (d), the A-site atom is always placed at the cell origin so that comparison of P_{el} at different lattice constants is meaningful. Also because the system is charge neutral, the cancellation of P_{el} and P_{ion} does not depend on the choice of the origin. Inset of (d) shows the fine structure of Ti-O2 and Ti-O3 bond lengths versus the in-plane (a) constant.

When the in-plane lattice constant is further decreased to 3.70 Å, another unusual phenomenon takes place in Fig. 2(a); the strain-induced change in χ_3 drastically slows down and the χ_3 quantity eventually saturates at a value of 1.05. Further increase in the in-plane strain ceases to influence the χ_3 value. Since change in polarization is known as a complex phenomenon caused by collective interaction, the predicted χ_3 saturation suggests the existence of a notable and sophisticated physics in the large-strain regime. The saturation also reveals that there is a profound limit that the χ_3 quantity cannot exceed, despite that large in-plane strain is applied. We have also performed polarization calculations for BT and ST; results are given in Fig. 2(b). Figure 2(b) shows that (i) the existence of a three-stage polarization response and (ii) the saturation of the χ_3 polarization, apply to all three substances, thereby demonstrating a general phenomenon. Also interestingly, we find that χ_3 saturates at similar values in BT and in ST but differently in PT. By saturation of χ_3, the proper piezoelectric e_{31}^{pro} coefficient vanishes and meanwhile the c-axis polarization $P_3 = \frac{e}{\Omega}\chi_3 c = \frac{e}{a^2}\chi_3$ is altered only because the external strain forces the a lattice constant to decrease (therefore P_3 follows a scaling law $P_3 \sim \frac{1}{a^2}$). To verify whether the χ_3 saturation is applicable to FEs other than the titanate family, we have further calculated the strain dependence of the polarization in tetragonal $BiScO_3$, and find that the χ_3 quantity also saturates, at a rather small in-plane strain of 2.5%.

The χ_3 saturation cannot be naively attributed to the saturations of effective charges and/or atomic displacements. We

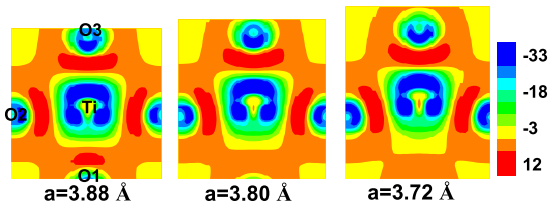

FIG. 3. (Color online) Charge-density difference $\Delta\rho=\rho-\rho_0$ in units of $1/\text{Å}^3$, where ρ_0 is the sum of electron density of free atoms, in PT at three different in-plane lattice constants of $a=3.88$, 3.80, and 3.72 Å. The plotted density is on the plane that cuts through the Ti, O1, O2, and O3 atoms.

see previously in Fig. 1(b) that the O displacements do not saturate, in fact. To examine if effective charge saturates, we compute the effective Z^*_{33} charges of different ions in strained PT, by finite difference $Z^*=\frac{\Omega}{e}\frac{\Delta \mathbf{P}}{\Delta \mathbf{r}}$. Under zero strain, the calculated effective charges (denoted as Z^*_0) are 3.65 (Pb), 5.76 (Ti), −4.90 (O1), and −2.28 (O2). With the impose of strain, we are interested in the change in the effective charge, namely, $|Z^*|-|Z^*_0|$, which is given in Fig. 2(c). Note that whereas polarization increases once compressive strain is applied, the effective charges nevertheless decrease as revealed in Fig. 2(c). We also recognize that the $|Z^*|-|Z^*_0|$ in Fig. 2(c) separate into two groups: one group consists of Ti and O1 atoms and the other Pb and O2 atoms. The strain dependence of the effective charge is similar within each group, implying the existence of a correlation arising from chemical bonding. Furthermore, Fig. 2(c) shows that Z^*s do not saturate. For instance, the Z^*_{33} of Pb (also of O2) slightly increases when a is below 3.7 Å. Since $\delta\chi_3=\Sigma_i\{\delta Z^*_i\Delta r_{i,z}+Z^*_i\delta(\Delta r_{i,z})\}$ (where i is the atom index), the saturation in χ_3 must result from a delicate cancellation between strain-induced variations in Z^* and of atomic displacements. In BT and ST, while Ba or Sr has less hybridization with O than Pb, this difference exists primarily when materials are near their respective equilibrium. At large in-plane strains, the A-O bond length becomes short and the Z^* charges in BT and ST behave similarly as in PT.

V. MICROSCOPIC INSIGHT AND IMPLICATION OF POLARIZATION SATURATION

We now provide possible microscopic explanations on why polarization undergoes the puzzling change from stage I to stage II and why χ_3 saturates at stage III of high strains, by studying electron density which is shown in Fig. 3. The same contour interval and color code are used in Fig. 3 for different strains; comparison of relative intensity is thus meaningful. Not surprisingly, the electron distribution in equilibrium PT is as expected; charge transfer leads to electron deficiency near atomic cores (blue regions, color online) while more electrons accumulate in the interstitial area between atoms (red regions, color online). As PT is strained to $a=3.80$ Å, a significant change occurs, namely, the overlapping charge largely disappears between Ti and O1 atoms. The considerably weakened Ti-O1 bond makes it easier for the Ti atom to move off center and toward the O3 atom. The broken Ti-O1 bond is thus responsible for the enhanced tetragonality in stage II.

When PT is further strained to $a=3.72$ Å, the (blue-colored online) electron density near the O3 atomic core is evidently deformed and no longer has the half-spherical shape as in $a=3.88$ Å. Also note that the distorted shape of the density near the O3 core bears a resemblance to the shape of the (red-colored online) electron density in the interstitial region between Ti and O3, showing that the electrons in these two regions are considerably coupled due to Coulomb interaction. Since the electrons near the O3 nuclei interact strongly with the O3 ion (while coupling to the bonding charge between Ti and O3 as described above), we thus anticipate that ionic displacement and electron deformation (both contributing to the total polarization) are to be correlated. This correlation should reflect itself in the electronic (P_{el}) and ionic (P_{ion}) contributions to the total (P_{tot}) polarization, and is indeed born out in Fig. 2(d). When a decreases between 3.88 and 3.70 Å, P_{el} rises faster than the declining P_{ion}, giving rise to an overall enhancement of the total polarization. However, when a is below 3.70 Å, the P_{el} and P_{ion} contributions show equal slopes but opposite signs, which confirms the above-described electron-ion correlation and which leads to the predicted polarization saturation in stage III. Another indication of the strong electron-ion correlation is manifested by the fine structure of the Ti-O3 bond length [see the inset of Fig. 2(d)]. We find that when χ_3 starts to saturate near $a=3.70$ Å, the Ti-O3 bond length begins to increase notably. From our calculations, the minimum length by which the Ti-O3 short bond can be compressed is found as 1.76 Å (PT), 1.78 Å (BT), and 1.79 Å (ST). Reaching this minimum bond length implies the onset of polarization saturation. Here we should point out that more accurate methods such as Quantum Monte Carlo or LDA+U may be needed to describe the electron-electron correlation when in-plane strain is large. However, for the reasons to be described below, we believe that our conclusion on the strain-induced saturation of polarization is likely to remain. First, LDA generally fails for strongly correlated systems with partially occupied d or f orbits. But our systems do not have partially occupied orbits and we find that PT at 5% in-plane strain remains to be an insulator with an LDA gap of more than 2 eV. Second, the lengths of Ti-O2 and Ti-O3 bonds subject to very little changes at large strains [Fig. 1(c)], suggesting that wave-function overlap is modified but not to the degree that the use of LDA+U method will drastically alter the conclusion.

Our calculations are consistent with and/or provide understanding to the results of previous theoretical studies and experimental measurements.[5,18] (i) Recently, a significant enlargement in electromechanical response was observed in PZT films when these films are under very large (~200 MV/m) electric fields.[18] We believe that the enhanced c/a region between A and B predicted in Fig. 1(a) provides an explanation for this observation since high electric fields drive the films into the large strain regime. More recently, a theoretical study using first-principles calculations under constrained electric displacement was performed for PZT under finite electric fields,[26] showing that electric fields within the experimental range can indeed give rise to large piezoelectric response. (ii) Our calculations explain why highly strained PZT films exhibit a surprisingly weak strain-

dependent polarization as observed in Ref. 5. This is because the PZT films, when strained to the lattice constant of ST substrate, are in the regime of polarization saturation. The experimental observations in Refs. 5 and 18 thus provide rather convincing evidence for the validity of our theory, particularly on the strain-induced polarization saturation. (iii) Our study also provides a unified picture, naturally explaining why some FEs display large-strain-induced polarization enhancement while other FEs do not. FEs with sensitive strain-dependent polarization include PT and BT as revealed in Ref. 4. On the other hand, $BiFeO_3$ and $LiNbO_3$ (as shown in Ref. 4) and PZT (as shown in Ref. 5) yield a very weak dependence of polarization on compressive in-plane strain. The difference could be simply explained by the fact that these materials of zero strain are in different stages of the polarization-response curve. Strain-sensitive materials (PT, BT, etc.) have a zero-strain equilibrium structure which lies in stage I or II of the polarization-response curve. Those strain-insensitive substances ($BiFeO_3$, $LiNbO_3$, and $BiScO_3$) instead are within or near stage III of saturated polarization.

Further test of the χ_3 saturation is also possible. According to our calculations, the χ_3 saturation occurs at an in-plane strain of ~4.5% in PT and at ~6.5% in BT or ST. These strains are moderate and might be realized in FE nanowires of intermediate size range (e.g., 10–50 nm in diameter). In fact, molecular-dynamics simulations of ZnO nanowires indicated that nanowires can sustain strains up to 7% before mechanical failure.[11] Furthermore, we note that the χ_3 saturation occurs at relatively small strains in epitaxially grown $BiScO_3$ (with a saturation strain at ~2.5% as revealed by our calculations) or in PZT (as hinted by the measurement result in Ref. 5). Our theory can thus be more conveniently tested in $BiScO_3$ or PZT using thin films. Meanwhile, one should bear in mind that surface of nanostructures, in addition to in-plane strain, may also affect the polarization.

VI. STRAINED STRONTIUM TITANATE WITH OXYGEN ROTATION

Thus far we have restricted the structure of strained perovskites to be tetragonal, without allowing the rotation of the oxygen octahedra. It is known that in unstrained ST the oxygen octahedra rotate around the c axis to reduce the total energy. Under small compressive in-plane strains, the rotation angle of the octahedra tends to increase in order to accommodate the strain, which often leads to the reduction in the c-axis cell length. However, at moderate and/or large strains, evolution of this rotation and its effect on the c-axis polarization remain less known. One question of interest is whether the polarization still saturates at high strain with the presence of this rotation. We hereby determine the structure of compressively strained ST by allowing the rotation of the oxygen octahedra and study the polarization response of the material. For this purpose, a unit cell of 10 atoms is used. For a given in-plane lattice constant, we choose different c/a ratios and determine total energy and optimized atomic positions.

The total energy as a function of the c/a ratio is shown in Fig. 4(a) for selected in-plane lattice constants. Notice that when in-plane lattice constant is between 3.67 and 3.59 Å,

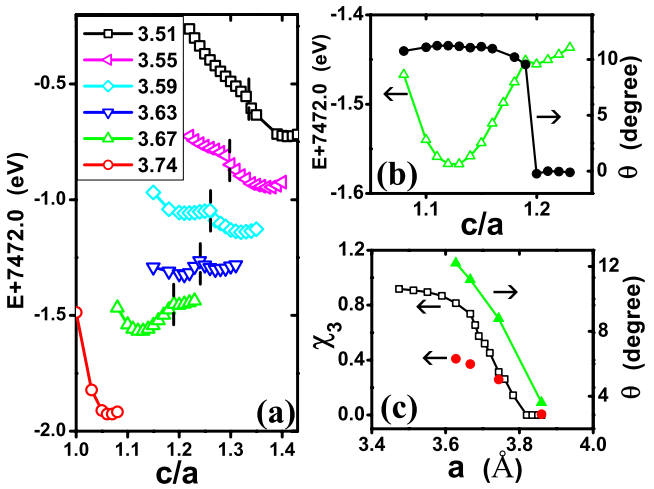

FIG. 4. (Color online) Properties of strained ST with oxygen-octahedra rotation allowed in the calculations: (a) Dependence of the total energy of a 10-atom cell, as a function of c/a. Different curves correspond to different in-plane lattice constants. (b) Rotation angle θ (solid circles, using the right vertical axis) and the total energy (empty triangles, using the left vertical axis) as a function of c/a, for in-plane lattice constant $a=3.67$ Å. (c) Calculated χ_3 values (using the left vertical axis) in strained ST with (solid circles) and without (empty squares) oxygen rotation, as a function of in-plane lattice constant. The optimized rotation angle (solid triangles, using the right vertical axis) is also given. When $a<3.61$ Å, the cell structure with oxygen rotation is no longer stable and the χ_3 quantity in ST will resume the value described by the curve of empty squares.

the energy curve displays two local minima, located at different c/a ratios. The most stable structure that corresponds to the lowest energy shifts from the first minimum with a smaller c/a ratio to the second one with a larger c/a ratio when the in-plane a lattice constant decreases. Meanwhile, only the second energy minimum survives for $a=3.55$ and $a=3.51$ Å. For $a=3.74$ Å, only the first energy minimum exists. To understand the origins of the two energy minima, we show in Fig. 4(b) the rotation angle θ of the oxygen octahedra as a function of c/a, for $a=3.67$ Å. We see that for the first energy minimum, the rotation angle is 11°, and this rotation angle does not change appreciably when we vary the c/a ratio in the nearby of the energy minimum. However, as the c/a ratio increases to ~1.2, the rotation angle suddenly drops to zero. It is thus clear that the second energy minimum corresponds to a crystal structure without oxygen rotation. Similar discontinuity in the θ angle as a function of c/a has also been observed for other in-plane lattice constants and the transition point for the structure to change from rotational to nonrotational is marked by a short vertical line in Fig. 4(a). An abrupt change in the energy curvature is evident at the transition point. Therefore, for a given in-plane lattice constant a, with the increase in the out-of-plane length c, a first-order structural transition occurs, featured by the sudden change in the structure symmetry. For $a=3.74$ Å, we did not draw in Fig. 4(a) the energy curve for the nonrotational structure since the energy is rather high and overlaps with another curve. The calculation

results in Figs. 4(a) and 4(b) can be understood as follows. While we apply compressive in-plane strains in ST, the material has two ways to lower the system energy, by rotating the oxygen octahedra and by increasing the out-of-plane c length. At small strains, the octahedral rotation is more effective and it leads to a smaller c/a ratio due to the coupling between oxygen rotation and tetragonal strain. However, at large strains (i.e., $a<3.61$ Å), the relaxation channel due to oxygen rotation is no longer effective and is replaced by the channel of the out-of-plane tetragonal strain, resulting in a structure of no oxygen rotation. By comparing the atomic positions and c/a ratio, the zero-rotation crystal structure of the second minimum in Fig. 4(a) for 10-atom cell is the same structure as we have obtained in Sec. III for 5-atom cell. As a result, all our calculation results of strained ST in Secs. III and IV remain unchanged for large in-plane strains ($a<3.61$ Å).

In Fig. 4(c) we report the χ_3 component of the polarization and optimized rotational angle in strained ST when the oxygen-octahedra rotation is stable (i.e., $a>3.61$ Å). The χ_3 values in strained ST, when there is no oxygen rotation, are also given for comparison. With rotation, ST has a smaller c lattice constant as seen in Fig. 4(a) and thus a smaller χ_3. However, when a is below 3.61 Å, the system prefers a structure with no oxygen rotation so our previous result on the χ_3 saturation remains to be valid. At zero strain, our LDA calculations yield a rotation angle of 3.6°, which is slightly larger than the experimental value of 2.1°.[27] Another first-principles calculation gives the rotation angle of 5.5°.[28] With the application of compressive in-plane strain, the rotation angle increases substantially, reaching a value of ~13° at $a=3.63$ Å.

VII. SUMMARY

Density-functional calculations on compressively strained FEs reveal several notable phenomena in the intermediate and large-strain regimes: (1) a notable nonmonotonous change in cell volume, (2) occurrence of strongly enhanced c/a tetragonality and ferroelectric off-center displacements for the intermediate strains between A and B, (3) increase in rotation angle in ST at small strains and disappearance of the oxygen rotation at large strains, (4) the saturation of the χ_3 polarization upon high strains, and (5) χ_3 saturates in all three considered materials, thus being a general principle. As another outcome of this study, we identify the microscopic origins responsible for these properties. The enhanced piezoresponse and the enlarged c/a tetragonality in stage II are associated with the weakening of the Ti-O1 bonds and the expansion of the cell volume. The continuous transition from stage I to II may produce marked piezoelectric responses. On the other hand, strong electron/ion correlations lead to the cancellation of electronic and ionic polarizations, resulting in the polarization saturation at stage III. Our calculations reveal the existence of a limit beyond which the χ_3 polarization cannot exceed by mechanical in-plane strains.

ACKNOWLEDGMENTS

This work was supported by the Office of Naval Research. We thank H. Krakauer and D. Vanderbilt for very useful discussions.

[1] K. M. Rabe, Curr. Opin. Solid State Mater. Sci. **9**, 122 (2005).
[2] D. G. Schlom, L.-Q. Chen, C.-B. Eom, K. M. Rabe, S. K. Streiffer, and J.-M. Triscone, Ann. Rev. Mater. Res. **37**, 589 (2007).
[3] M. Dawber, K. M. Rabe, and J. F. Scott, Rev. Mod. Phys. **77**, 1083 (2005).
[4] C. Ederer and N. A. Spaldin, Phys. Rev. Lett. **95**, 257601 (2005).
[5] H. N. Lee, S. M. Nakhmanson, M. F. Chisholm, H. M. Christen, K. M. Rabe, and D. Vanderbilt, Phys. Rev. Lett. **98**, 217602 (2007).
[6] K. J. Choi, M. Biegalski, Y. L. Li, A. Sharan, J. Schubert, R. Uecker, P. Reiche, Y. B. Chen, X. Q. Pan, V. Gopalan, L.-Q. Chen, D. G. Schlom, and C. B. Eom, Science **306**, 1005 (2004).
[7] J. H. Haeni *et al.*, Nature (London) **430**, 758 (2004).
[8] A. Antons, J. B. Neaton, K. M. Rabe, and D. Vanderbilt, Phys. Rev. B **71**, 024102 (2005).
[9] J. F. Scott, Science **315**, 954 (2007).
[10] Y. Duan, H. Shi, and L. Qin, J. Phys.: Condens. Matter **20**, 175210 (2008).
[11] A. J. Kulkarni, M. Zhou, and F. J. Ke, Nanotechnology **16**, 2749 (2005).
[12] J. J. Urban, W. S. Yun, Q. Gu, and H. Park, J. Am. Chem. Soc. **124**, 1186 (2002).
[13] N. Reyren *et al.*, Science **317**, 1196 (2007).
[14] B. Dkhil (private communication).
[15] D. Vanderbilt, J. Phys. Chem. Solids **61**, 147 (2000).
[16] G. Saghi-Szabo, R. E. Cohen, and H. Krakauer, Phys. Rev. Lett. **80**, 4321 (1998).
[17] S. Tinte, K. M. Rabe, and D. Vanderbilt, Phys. Rev. B **68**, 144105 (2003).
[18] A. Grigoriev, R. Sichel, H. N. Lee, E. C. Landahl, B. Adams, E. M. Dufresne, and P. G. Evans, Phys. Rev. Lett. **100**, 027604 (2008).
[19] P. Hohenberg and W. Kohn, Phys. Rev. **136**, B864 (1964); W. Kohn and L. J. Sham, *ibid.* **140**, A1133 (1965).
[20] H. Fu and O. Gulseren, Phys. Rev. B **66**, 214114 (2002); H. Fu, in *Fundamental Physics of Ferroelectrics*, edited by R. E. Cohen (AIP, New York, 2002), p. 17.
[21] N. Troullier and J. L. Martins, Phys. Rev. B **43**, 1993 (1991).
[22] Details were given in Ref. 20 and in I. I. Naumov and H. Fu, Phys. Rev. B **72**, 012304 (2005); Z. Alahmed and H. Fu, *ibid.* **76**, 224101 (2007).
[23] R. D. King-Smith and D. Vanderbilt, Phys. Rev. B **47**, 1651 (1993).
[24] R. Resta, Rev. Mod. Phys. **66**, 899 (1994).
[25] M. E. Lines and A. M. Glass, *Principles and Applications of Ferroelectrics and Related Materials* (Clarendon, Oxford, 1979).
[26] M. Stengel, N. A. Spaldin, and D. Vanderbilt, Nat. Phys. **5**, 304 (2009).
[27] E. Courtens, Phys. Rev. Lett. **29**, 1380 (1972).
[28] N. Sai and D. Vanderbilt, Phys. Rev. B **62**, 13942 (2000).